Postprint of: Balewski L. et al., Step on It Bringing Fullwave Finite-Element Microwave Filter Design up to Speed, in IEEE Microwave Magazine, vol. 21, no. 3 (2020), pp. 34-49, DOI: 10.1109/MMM.2019.2958165

Step on it! Bringing Fullwave Finite-Element Microwave Filter Design up to Speed

Lukasz Balewski, *Member, IEEE*, Grzegorz Fotyga, *Member, IEEE*, Adam Lamecki, *Senior Member, IEEE* Michal Mrozowski, *Fellow, IEEE*, Martyna Mul, *Student Member, IEEE*, Piotr Sypek, and Damian Szypulski, *Student Member, IEEE*

There are many steps in the design of a microwave filter: mathematically describing the filter characteristics, representing the circuit as a network of lumped elements or as a coupling matrix, implementing the distributed elements, finding the initial dimensions of the physical structure, and carrying out numerical tuning using electromagnetic simulators. The whole process is painstaking and time-consuming, and requires a great deal of engineering expertise. Microwave filters are very complex geometric structures and their simple circuit representation is often very hard to find. Moreover, manufacturing them is costly, so in order to be sure that the hardware resulting from the design will meet the performance goals, rigorous computer tools are used to determine the physical dimensions and to evaluate all the adjustments at the final stage. This last stage is particularly challenging, and advanced computational techniques are required.

At microwave frequencies, the physics governing the operation of a filter are given by Maxwell's equations. To accurately predict a filter's behavior, the software has to numerically solve Maxwell's equations at all frequencies, within a given frequency band, and with high accuracy. There are several methods that are used in commercial and in-house code to do this, including the method of moments, mode matching, the finite-difference method, and the finite-element method. Unfortunately, all electromagnetic (EM)-based solvers have the same problem of long computation times. During the numerical tuning and final global optimization stages, the simulations must be repeated many times. Waiting for design closure can be frustrating.

In an ideal world—or at least in a microwave filter designer's paradise—it would be as simple as providing the filter specifications, clicking *START*, and letting the computer do all the work. The humans involved would relax and have more time to enjoy life and develop themselves, while the machines did all the chores. This designer's paradise is still far away, and in fact may never be reached: humans will always need to make some knowledgeable decisions on filter topology and implementation, even if the tedious task of refining the crude design to meet performance goals can be left to the machine. In theory, this can be achieved using computer-aided design (CAD) tools that are meant to assist an engineer by design-by-optimization. To date, running complex optimization tasks based on full-wave solutions of Maxwell's equations has been considered infeasible, especially when the number of design variables is large and the initial design is not high enough quality. In 2007, *Microwave Magazine* ran a feature article by microwave filter experts Dan Swanson and Giuseppe Macchiarella [1], who remarked: "without a good starting point, the most elegant optimization procedure may not be able to find an acceptable solution." More recently, in 2011, also in a feature article in *Microwave Magazine*, Ming Yu and Ying Wang [2] observed: "a brute force application of optimization, for example by defining a cost function based on the specification and feeding it to an optimizer, is rarely successful."

As we will see, recent advances in computational electromagnetics and CAD mean that these two statements are likely to need revision: to a large extent, designers' dreams may soon come true. The answer to these dreams lies in overcoming a few crucial obstacles, which we will discuss in detail in this paper. We focus on the design-by-optimization of filters using electromagnetic solvers based on the finite-element method (FEM) [3], [4], as this is one of the most general and powerful numerical techniques, and one which is ideally suited to the arbitrarily shaped 3D geometries found in many microwave filter implementations. With suitable enhancements, FEM can address many of the challenges that have prevented successful EM-based CAD of microwave filters. Moreover, while the focus of this article is on FEM, some of the techniques we describe also apply to other full-wave methods.

The most important factor for designers is the overall time needed to complete a design. Since a single full-wave simulation takes a long time, one way to speed up the process is to use a full-wave solver as little as possible—maybe just a few times in the entire design cycle–to verify if the design obtained from faster, less accurate approaches is good enough. Thus a variety of techniques that operate with two (or more) mathematical models of a microwave structure have been proposed. The first of the two models is simplified, but can be evaluated very quickly, and crucially often gives sensitivities with respect to the design parameters. This allows designers to use gradient-based optimizers. Using a simplified model, the optimizer converges to an approximate solution, and the accuracy of the design is verified against a second

L. Balewski and A. Lamecki are with EM Invent, Gdańsk, Poland (http://www.eminvent.com); G. Fotyga, A. Lamecki, M. Mrozowski, M. Mul, P. Sypek, and D. Szypulski are with the Faculty of Electronics, Telecommunications, and Informatics, Gdańsk University of Technology, Poland (e-mail: lukasz.balewski@eminvent.com, grzfotyg@pg.gda.pl, adam.lamecki@eminvent.com, m.mrozowski@ieee.org, martyna.mul@pg.edu.pl, psypek@eti.pg.edu.pl, damian.szypulski@pg.edu.pl).

The "EDISOn - Electromagnetic Design of flexIble SensOrs" project, agreement no POIR.04.04.00-00-1DC3/16-00, is carried out within the TEAM-TECH programme of the Foundation for Polish Science co-financed by the European Union under the European Regional Development Fund, Smart Growth Operational Programme 2014-2020.

(costly) high-fidelity model. This shows how the crude model can be corrected to improve its accuracy. The whole process is then repeated. There are various ways to create a low-fidelity model and subsquently improve it. The model can take the form of an equivalent circuit of a structure—or of a mathematical multiparametric surrogate metamodel that has been constructed upfront—or it may be purely numerical, provided by the same solver as the high-fidelity approach, though executed with relaxed accuracy settings. In surrogate-based optimization, the metamodel can be constructed using a response surface [5], through kriging [6], [7], or by using radial basis function [8] interpolation techniques. Artificial neural networks [8]–[10] and extreme learning techniques [11] have also been described. If we want to improve model quality, we can use either sample-point refinement (where the model is augmented with new samples around the optimum) or various space-mapping approaches (such as input, output, implicit, and aggressive manifold mapping). These approaches have been successfully employed to conduct efficient and highly accurate EM-based design optimization [12]–[14]. They have also often been used in other areas of engineering when evaluating the response would take too long [15]–[17]. When designing filters using FEM, exceptionally good results have been obtained with multifidelity (two-level) manifold mapping with frequency correction [18] where, for a fifth-order linear-phase filter involving as many as fifteen design variables, as well as two complex and two imaginary transmission zeros, only three high-fidelity model evaluations (and just one set of derivatives on the fine level) were needed to reach the design specification, starting from a very poor initial design.

Besides these ideas, remarkably fast optimization can also be carried out by directly running full-wave solvers. In the remainder of this paper, we will discuss only this approach and show some ways to reduce runtime. We used InventSIM for all the numerical examples; this is a commercial FEM simulation and optimization framework [19] that implements many of the techniques that we discuss in this paper. Other commercial FEM tools, including ANSYS HFSS and CST Studio Suite® (Frequency Domain Solver), also provide features that can speed up computations. Both CST Studio Suite® and InventSIM offer special modules intended to expedite microwave filter designs.

I. Under the hood: the finite-element method

To understand the key factors affecting the speed and accuracy of EM-based CAD of microwave filters, we will first recall the basics of the finite-element method and of the numerical techniques for finding a solution. In FEM, a partial differential equation governing the physics underlying the problem (a wave equation in electromagnetics) is converted into a system of linear equations [3], [4]. To this end, the entire domain of interest is meshed; the most popular shape in three dimensions is tetrahedral. In each tetrahedron, the field is represented as a linear combination of basis functions with unknown coefficients. To find these coefficients, the wave equation is first converted to the weak form, and the Galerkin procedure is then applied with the basis functions that are also used for testing. Boundary conditions are applied at this stage too. This process results in a large system of equations with the unknowns—referred to as degrees of freedom (DoF)—being the coefficients of the basis functions in each tetrahedron. It is important to note that the number of DoF is large, but the coefficient matrix for the system of equations is sparse. In practice, the matrix can have over one million rows and columns, with about 20 nonzero elements per row. The matrix is usually symmetric, but may be complex-valued. Once the system has been solved, the EM field can be found inside the structure, and processing this field at the ports yields the scattering matrix needed to represent the properties of the microwave filter.

A typical simulation scenario involves setting up the mesh and solving the resulting sparse system of linear equations for each frequency of interest. For better accuracy, the mesh is created in an adaptive way, beginning with a low-resolution mesh and moving to increasingly refined ones. At each iteration, the local error in the mesh is monitored and the mesh density is increased in the critical areas. To find the best mesh for a given problem, it is necessary to repetitively solve the system of FEM equations with an increasing number of DoF in each iteration; this is a rather time-consuming process.

This brief outline of FEM is intended to provide a background for the approaches to accelerating EM-based CAD. The most time-consuming of these is to solve a system of FEM equations with the form:

$$\begin{aligned}(\Gamma + sG + s^2C)E(s) &= sBI,\\ U &= B^TE(s),\end{aligned} \tag{1}$$

with the transfer function (which is the impedance matrix) defined as follows:

$$Z(s) = B^H(\Gamma + sG + s^2C)^{-1}sB. \tag{2}$$

In this system of equations, Γ, G, and C are FEM system matrices with n rows and columns, B is the normalized $n \times m$ port selection matrix, where n and m are the number of DoF and the number of ports, respectively; finally, $s = j\omega/c$ is the complex frequency, and c is the speed of light.

The system of equations (1) is solved many times during the simulation process: initially during mesh adaptation and then during the frequency sweeps, when a solution has to be found at each frequency point. Let's look at this step in more detail: for moderate-sized systems, with up to 3 or 4 million DoF and a workstation with about 64 GB of RAM, the fastest way to find a solution will be to use a direct method. In a direct method, the coefficient matrix is factorized. Because storing the factors requires much more memory than storing the matrix, factorization is performed in two stages. The first stage is symbolic factorization, the goal of which is to determine the nonzero pattern for the factors and to permute the rows and columns in such a way that the factors occupy the least memory. The factors are computed in the next stage, called numerical factorization. Using the factors, the solution can be found very rapidly. Fig. 1 shows pie charts with the fraction of time spent in each stage, for two cases, with the problem solved at 1 or 101 frequency points, respectively. Two

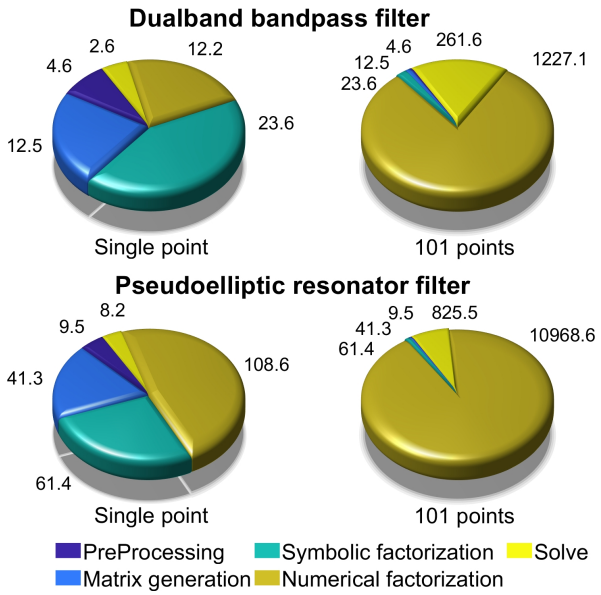

Fig. 1. Pie charts showing the time spent on each stage of the FEM process, with the problem solved at 1 and 101 frequency points, respectively. Two filters are shown, with FEM problems with about 1.4 and 3.5 million DoF.

filters are considered, generating FEM problems with about 1.4 and 3.5 million variables (see Section II for details). It is evident that factorization is the most time-consuming element, so it should be done as infrequently as possible. It is also important to remember that the symbolic factorization results can be reused as long as the size and sparsity pattern of the matrix do not change. This happens during frequency sweeps, so the symbolic factorization is performed only once during the process. However, if we analyze the filter at nF points using a so-called discrete sweep, we have to carry out the numerical factorization nF times. This number can be large if we are trying to resolve fine filter features like the location of transmission and reflection zeros, or to carry out wideband analysis so as to find a spurious passband.

II. Fast Frequency Sweep

It should be remembered that EM-based CAD with an FEM simulator involves numerical optimization requiring at least several iterations for design closure. This means that, in order to design a filter, we need to perform FEM simulations repeatedly, each time calculating the filter response at many points in the frequency band of interest. One way to reduce the total time needed for the design is to perform the frequency sweeps as fast as possible. The simplest way to carry out a fast frequency sweep is to use the results of the EM analysis at a few frequency points to gather data for interpolation, in an approach called an interpolating sweep. The response of the EM system can be approximated by a rational function [20]. A rational interpolant can be found by means of the Cauchy method [21], [22], the Bulirsch–Stoer algorithm [23], [24], vector fitting [25], or a Loewner matrix [26], [27].

Interpolating sweeps with adaptive sampling greatly reduces the number of matrix factorizations. However, there are other approaches that can result in even greater time savings. These make use of the concept of model-order reduction (MORe). The basic idea here is to replace the original complex model with a much simpler reduced-order model (ROM) that retains the original features with sufficient accuracy. Rational interpolation is one way to create these models. Here we are concerned only with finding a compact representation of the input–output behavior of our system within the desired band and do not get any information regarding the EM field at frequencies other than interpolation nodes. This is a data-driven MORe [28]. The other technique, model-driven MORe, gives us both the transfer function and the field. At the heart of a model-driven MORe lies the assumption that the EM field inside a structure (here a filter) at any given frequency can be expressed as a superposition of a small number of orthogonal vectors. The idea behind this can be understood intuitively. If we consider the field distributions inside the structure at two frequencies close to each other, we expect them to be "similar." Going one step further, if we were to collect all the field solutions within a frequency range and determine how linearly independent they are (this can be done numerically by computing the singular value decomposition (SVD) of the block matrix containing all the collected field samples), we would discover that, indeed, they can all be expressed as a linear combination of a small number of orthogonal vectors. These vectors form the basis of a linear subspace in which all possible field solutions for a given band reside. If by Q we denote the block matrix composed of r orthogonal basis vectors $q_i, i = 1 \cdots r$ for this subspace, then any field within this frequency range could be expressed as:

$$E(s) \approx QE_r(s). \tag{3}$$

All that remains is to find the expansion coefficients $E_r(s)$. The Galerkin method can be used to project the original system of FEM equations (the full-order model or FOM) onto a subspace spanned by the basis Q.

The projected system is solved for each frequency, yielding a vector of coefficients $E_r(s)$ of the frequency-dependent coefficients. Since the projected system has a size $r \times r$ and $r \ll n$, with n being the number of DoF in an FOM, the frequency sweep can be performed extremely rapidly.

The choice of the basis is not unique. There are various model-driven MORe techniques that differ in how the projection basis Q is constructed. Intuitively, the simplest technique is called the reduced basis method (RBM), which samples the field at different frequencies. These samples or snapshots are then assembled in a matrix and the basis is computed directly via singular value decomposition. The location of the snapshots is elegantly determined using a greedy algorithm: the next snapshot is evaluated at the frequency point at which the current low-order model has the largest error [29]–[33]. A basis can also be constructed from a mixture of RBM snapshots and modal fields at resonant frequencies [34].

The second technique for finding the projection basis starts from the idea that the field can be expanded around a given frequency into a Taylor series. In the past, the coefficients for the expansion were computed in an explicit way, as with asymptotic waveform evaluation (AWE) [35]. Currently, this is done

in a more numerically stable manner through various moment-matching techniques. In these procedures, the resulting ROM has the property that, at a certain frequency (expansion point), the frequency derivatives of its transfer function agree up to a certain order with the derivatives of the transfer for the original full-order model. Many moment-matching techniques have been described, including the efficient nodal order reduction (ENOR) [36], the passive reduced-order interconnect macromodeling algorithm (PRIMA) [37], and the second-order Arnoldi method for passive order reduction (SAPOR) [38]. Other examples of moment-matching approaches are provided in [39]–[42]. Many researchers have demonstrated excellent results using moment-matching techniques for full-wave analysis of microwave devices [40], [43]–[47].

The moment-matching algorithms have the very desirable property that the matrix factorization only has to be performed at a single frequency point (expansion point). Yet this handy property cannot be used in wideband analysis of some microwave structures, such as components excited with dispersive transmission lines (e.g., microstrips, coplanar waveguides), or where the material properties depend on frequency (e.g., conductor loss). For such systems, either RBM-based techniques [33], [48] or multipoint moment-matching algorithms [49]–[53] are needed.

We have selected two examples that illustrate the time savings that can be obtained using various fast frequency sweep techniques. The first is a sixth-order in-line pseudoelliptic filter taken from [54]. The filter is excited with a coaxial line and consists of six dielectric resonators with coupling screws placed at an angle between the dielectric pucks, as shown in the inset to Fig. 2. The filter is narrowband and has its center frequency located at 2.17 GHz; two transmission zeros (TZs) are separated by 1 MHz. The simulations are carried out in a broader band (2–3GHz) in order to reveal spurious transmission bands. Due to the very narrow passband, and because the two transmission zeros are located very close to each other, this example is a challenge that requires a very high frequency resolution. The structure is closed, and we assume there is no dielectric or conductor loss. This means that the computations can be performed in real arithmetic. The second structure is a dualband bandpass planar filter designed to exhibit its lower and upper passbands centered at 0.63 and 2.37 GHz, respectively. The geometry of the structure is shown in Fig. 3 and described in detail in [55]. Here, we assume the structure is open, so the solver requires complex arithmetic. The wave port excitation is also used and, because the field pattern at the port changes with frequency, single-point moment-matching algorithms cannot be applied. In both examples, to emphasize the time savings resulting from fewer matrix factorizations, a rather fine mesh and higher-order basis functions are used, so that the FEM matrices are large (3.45 and 1.4 million DoF, respectively). We specified 0.1–3.0 GHz as the band for numerical analysis of the microstrip filter. For both filters, we first performed a discrete frequency sweep using the full-order FEM model. We used 501 equidistant points for the dielectric filter and 401 points for the microstrip filter. The computed characteristics and the time taken by the discrete sweep serve as reference results for assessing the

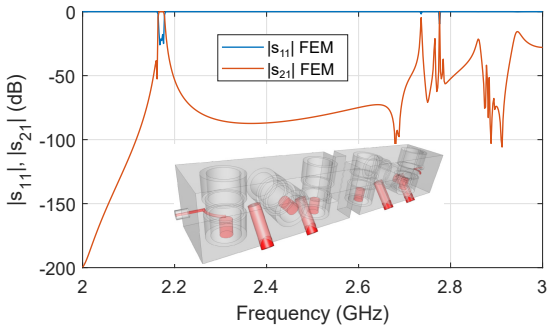

Fig. 2. Scattering parameters of the pseudoelliptic dielectric resonator filter.

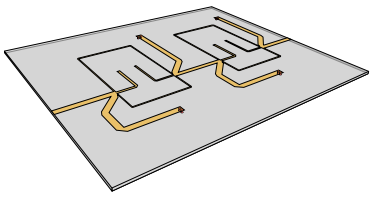

Fig. 3. A dualband bandpass planar filter [55].

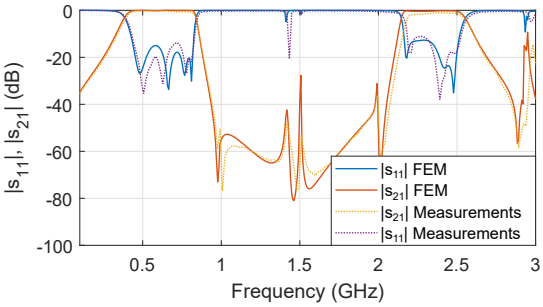

Fig. 4. Computed and measured scattering parameters of the dualband bandpass planar filter [55].

speed and accuracy of the fast frequency sweep algorithms. The computed characteristics are shown in Figs. 2 and 4. For the dualband filter, we plotted the measurements taken from [55].

We then ran simulations using various fast frequency sweep algorithms, including an interpolating sweep, RBM, and single or multipoint moment-matching model-order reduction techniques. Fig. 5 shows the CPU time for computations performed on a server with two Intel Xeon E5-2680 processors and 256 GB RAM. Two numbers are given on top of each bar: the first (in black) is the runtime in seconds, while the second (in blue) is the number of factorizations in each approach. It can be seen that fast sweeps can result in huge savings. For the pseudoelliptic filter, the runtime drops from almost 16 hours to 10 minutes 26 seconds, a 92-fold acceleration. For the dualband planar filter, the duration of the discrete sweep at 401 points is slightly less than 3 hours, while a fast sweep takes 5 minutes and 16 seconds, so the speedup is 32.5 times.

It is important to note that these speed gains do not mean that the accuracy is compromised. Projection-based (model-driven) MORe techniques take advantage of error estimators

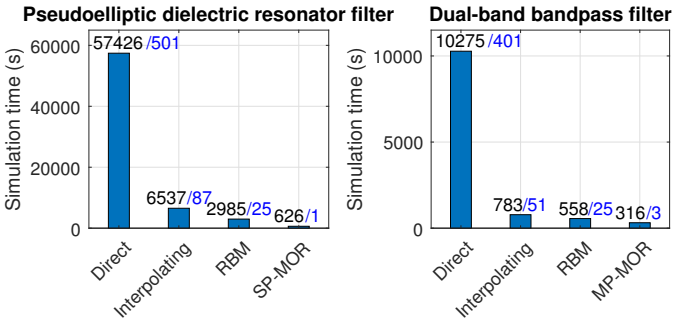

Fig. 5. Comparison of simulation runtime for both filters and selected frequency sweep methods. Numbers of factorizations are in blue. SP-MOR and MP-MOR stand for single and multipoint MOR, respectively.

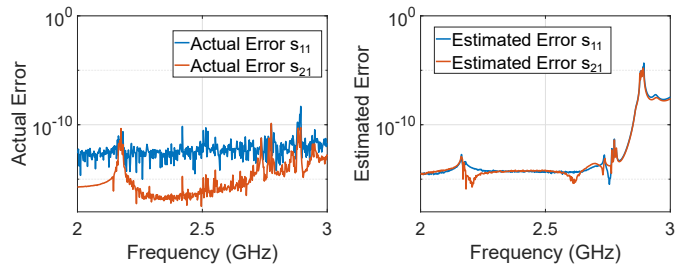

Fig. 6. Actual and estimated errors computed using SP-MOR for the pseudoelliptic dielectric resonator filter [54].

[29], [32], [56], [57], which are used as a stopping criterion, and also to control the size of the projection basis, or as indicators of frequency points at which the matrix should be factorized. Fig. 6 shows the estimated and actual errors for a moment-matching MOR. It is evident that machine precision has been achieved across the entire band, while the computations are almost two orders of magnitude faster.

III. Power Tools for the Microwave Filter Engineer

In the computer-aided design of microwave filters, the design goal is reached through many trials with candidate designs generated by an optimization algorithm. The design variables are geometric parameters, so the shape of the structure is modified from one iteration to another; it then has to be analyzed anew with FEM. The number of trials is large, so, for EM-based optimization, the time taken for each FEM simulation becomes crucial. If it is too long, the whole process will take forever and exhaust the patience of the engineer (and of the engineer's boss). Obviously, what counts in the end is the design quality and the time taken by the sum of all the computational steps, so the faster the convergence the better. The total number of iterations depends, among other things, on the optimization algorithms. Here we consider gradient-based optimization techniques that in general show the best convergence. These algorithms require the computation of derivatives, but this is not a problem, as the calculation of gradients in FEM with the adjoint sensitivity approach does not take long. An optimization algorithm itself does not guarantee success, even if many iterations can be afforded. There are two other aspects related to simulations that are crucial for successful EM-based CAD. One is the consistency of the results from one iteration to the next, and the second is the choice of the cost function to be minimized.

A. Fighting meshing noise and gaining additional speed boosts in the process

In many FEM packages that offer EM-based optimizations, the computational engine is simply called by an optimizer when the electromagnetic response needs to be calculated. The FEM engine itself has no memory of earlier simulations, and it is not aware of the optimization context. In each iteration, the optimization procedure calls the FEM engine with a modified structure, and the whole analysis starts again from scratch. This means that a new mesh has to be generated adaptively, and once it has converged, a new matrix must be set up, followed by at least one factorization. This brute-force approach not only involves redundant steps (mesh adaptation and symbolic factorization), but it can also cause poor convergence, or even a failure to converge.

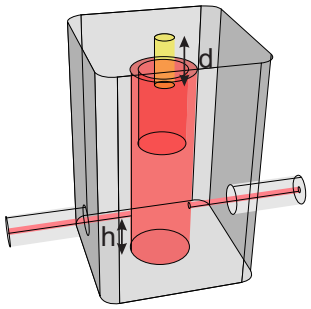

Fig. 7. A 3D view of a combline resonator fed with a coax line.

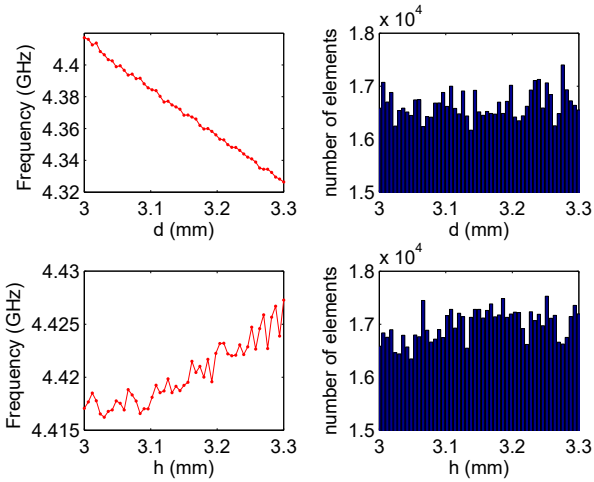

Fig. 8. Meshing noise in resonant frequency when changing combline resonator dimensions: screw length d (top) and feed height (bottom) with the corresponding number of mesh elements.

To see the pitfalls of decoupling the process of FEM analysis from optimization, consider how the resonant frequency of the combline resonator (Fig. 7) changes as we alter the length of the screw d. What we expect is a gradual change in the resonant frequency as d varies. Fig. 8 shows the results

of a series of FEM simulations performed independently of each other. For each value of the parameter d, we generated a mesh from scratch using several adaptation steps, in order to ensure that the results were accurate. Even though the mesh adaptation halts when the result converges, the meshes for two different lengths are completely uncorrelated (e.g., the mesh topology changes, which can be clearly seen when we consider the number of mesh elements, as shown in Fig. 9). This result is not what we would expect. The values computed with uncorrelated meshes follow a general trend, but do not lie on a straight line. A similar effect can be observed when other geometric parameters are modified. The same figure shows that changing the location of the feed point (h) leads to even higher variations in the resonant frequency, since a larger volume is affected by the parameter's change. This effect is called "mesh noise" and has sometimes been found to produce fictitious minima of the goal function, preventing convergence [58]. Mesh noise also introduces inconsistency into the results, both for the objective function and for its derivative with respect to geometric parameters from one point in the design space to another; these all act to mislead the optimizer. Gradient-based algorithms are particularly sensitive to mesh noise, and the number of iterations needed to reach a design goal depends strongly on the choice of parameters related to the gradient computation and on Hessian updates of the optimization procedure [59].

Mesh noise can be eliminated using mesh deformation (also called mesh morphing), where the mesh is dynamically modified as the geometry evolves: its nodes are relocated without changing the mesh topology. Fig. 9 illustrates this concept. As the inner hole moves, the original mesh (Fig. 9a) can be regenerated (Fig. 9b) or deformed (Fig. 9c). To account for the movement of the hole, the triangles above the hole are compressed, while those below are stretched; its number remains the same as in the original mesh (in this example, 196). In the remeshing approach, the new mesh has a different number of triangles (188).

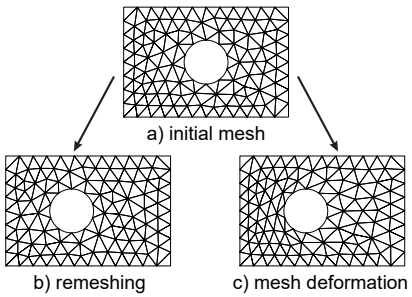

Fig. 9. Mesh deformation vs. remeshing while moving the inner hole. The original mesh and the deformed mesh have the same number of triangles (196), while the regenerated mesh has fewer elements (188).

Fig. 10 shows the results for the same problem, but this time using mesh morphing. It can be seen that the results are now nicely aligned, and no mesh noise is visible. The number of elements in the mesh is the same throughout the entire parametric sweep. Obviously, there is a certain numerical cost associated with mesh deformation, as the new position of each node has to be computed. The CPU time needed for this

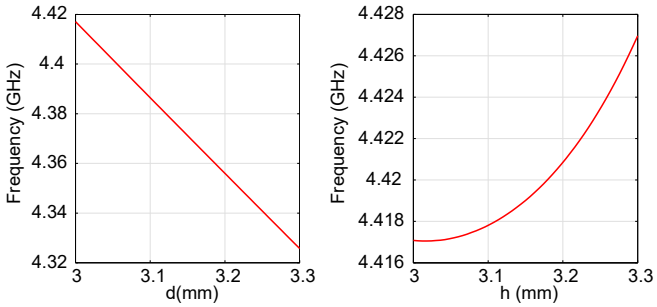

Fig. 10. Resonant frequency of the combline resonator vs. geometric parameters under mesh deformation.

process and the quality of the morphed mesh depend on the algorithm used. In general, the algorithms for mesh movement are either based on physical analogies (such as spring tension, elasticity, or Laplace's equation) or on interpolation (like inverse distance weighting, algebraic damping, or radial basis function interpolation) [60], [61]. Fast techniques—such as Laplacian smoothing [62], inverse distance weighting [63], and algebraic damping [64]—have only linear numerical complexity. Also, one nice thing about mesh morphing is that if a fast node movement algorithm is used, additional time savings are obtained, compared to shape optimization with uncorrelated meshes. First, there is no need to repeatedly generate and adapt a mesh. Next, since the mesh topology has not changed, the FEM matrix always has the same sparsity pattern, so the symbolic factorization is performed only once. Finally, the number of mesh nodes remains the same, so parametric model-order reduction techniques can be used [65].

Mesh deformation techniques for FEM-based optimization in electromagnetic problems were first considered over two decades ago [66], but little work has been published using this approach to analyze microwave devices [56], [67], [68]. We are aware of two commercial packages for microwave circuits that currently offer this feature (CST Studio Suite® and InventSIM). However, mesh deformation is often used in other engineering fields for shape optimization based on FEM.

B. Cost function

As noted above, computer-aided design is tantamount to solving an optimization problem with a suitably defined cost function. The cost function (called also the goal, error, or objective function) reaches its minimum when the design goals are met. The final two ingredients required for successful FEM-based design of microwave filters are the optimization algorithm and the cost function. When optimizing, fast convergence can be achieved using gradient-based techniques. With mesh deformation, the gradient needed for shape-optimization problems is consistent from one iteration to another, so we recommend this approach, even though the solution reached may be a local minimum. The cost function is extremely important and several choices are possible for filter design. The simplest cost function is constructed by selecting a number of frequency points within and outside of the band, and then computing either the absolute difference between the

simulated response at these points and their specifications [69] or dividing the desired value of the response at a given point by the computed result [70]. The optimization then minimizes the norm of a vector composed from these terms, possibly with weights, either in the least squares (L_2 norm) or min–max (l_∞ norm) sense [69]–[72]. The desired filter performance is usually described as a set of numbers providing the upper and lower bounds, imposed within a certain frequency interval on a given scattering parameter. Recently, a cost function built from feature points has been suggested [73], [74]. In filters, the frequency points corresponding to passband edges, transmission zeros locations, and local maxima of the reflection coefficient within the passband could be used as feature points. Frequency locations are used, rather than expecting the magnitude of the transmission or reflection characteristics to satisfy the requirements at many frequency points. The goal function is formed by taking the difference between the location of the feature points in the mathematical model of the filter and their location in the characteristics calculated by a simulator. A third (quite common) choice is a cost function involving the coupling matrix [75]–[78]. Here, the coupling matrix extracted from the simulated filter response is compared to the coupling matrix of a circuit model of the filter. Finally, there is a cost function based on the zeros and poles of the scattering parameters [79], [80].

IV. Does it work?

Now it is time to address the question of whether this designer's paradise will ever become a reality. Or is it perhaps just a pipe dream? Has computational electromagnetics reached a level of maturity where automated full-wave design of microwave filters—based entirely on electromagnetic FEM simulations—is feasible? To answer this, we selected three examples of passband filters with generalized Chebyshev responses. The level of difficulty increases from one example to the next.

A. Dual-mode waveguide filter

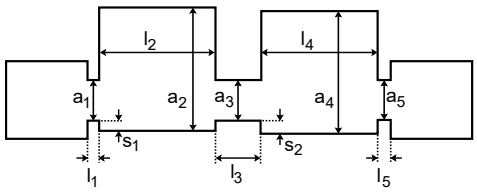

Fig. 11. Dual-mode waveguide filter.

The simplest of these filters to design is a dual-mode filter with two real transmission zeros [81] (Fig. 11). FEM simulations of this structure are quite fast: a single run with a fast frequency sweep takes about 30 seconds on a desktop computer. There are also only twelve design parameters. For this filter we will, however, perform a stress test and try to reach the specification, starting from various random designs. This will show whether we still need to carry out dimensional synthesis and whether a poor initial design will prevent the optimizer from reaching an acceptable minimum. Since the computations are rapid, we can afford to run many trials. In each one, a randomly selected starting point is used. We report the success rate and the number of iterations needed to reach the design goal. The numerical tests were constructed as follows: Three different sets of specification parameters were chosen (see Table I). For each specification, 100 trials were performed, each with random initial dimensions. For each trial, the number of iterations needed to reach the goal was recorded. If the optimizer did not converge–because one of the constraints was hit—we slightly extended the parameter range and ran the optimization for a second time. The range of the parameters considered in selecting the starting point, and then to explore the design space, is shown in Table II. Note that the allowed range for each design variable is quite broad, so an initial design may be quite far from the target.

TABLE I
Specifications of a dual-mode waveguide filter

	Design 1	Design 2	Design 3
f_c (GHz)	11.05	11.4	10.9
BW (MHz)	100	150	170
TZs (GHz)	10.95, 11.15	11.21, 11.57	10.70, 11.09
RL (dB)	20	20	20

TABLE II
Variation range of design parameters (dual-mode filter)

	min – max value (mm)		min – max value (mm)
a_1	8.5 – 10.8	l_1	2 – 3.2
a_2	28 – 31	l_2	25.5 – 30.5
a_3	8.8 – 11.2	l_3	10 – 12.5
a_4	27.8 – 31.5	l_4	27.2 – 31
a_5	8.8 – 11.2	l_5	2 – 3.8
s_1	2 – 3.5	s_3	1.5 – 3.2

Two objective functions were used for optimization. The first was the zero-pole objective function:

$$U(\mathbf{x}) = \sum_{i=1}^{N_p} |P^i_{11\text{spec}} - P^i_{11\text{resp}}|^2 + \sum_{i=1}^{Ntz} |Z^i_{21\text{spec}} - Z^i_{21\text{resp}}|^2 + \sum_{i=1}^{Nrz} |Z^i_{11\text{spec}} - Z^i_{11\text{resp}}|^2, \quad (4)$$

where $\mathbf{x}$ is the vector of design variables, P_{11}, Z_{11}, and Z_{21} are poles, reflection zeros, and transmission zeros, respectively, and N_p, Ntz, and Nrz are the number of poles, transmission zeros, and reflection zeros. The cost function is thus expressed as the difference between the poles and zeros of the ideal response ($P_{11\text{spec}}$, $Z_{11\text{spec}}$, $Z_{21\text{spec}}$) and the poles and zeros of the response in the k-th iteration ($P_{11\text{resp}}$, $Z_{11\text{resp}}$, $Z_{21\text{resp}}$). The second function, based on the scattering parameters, is defined as follows:

$$U(\mathbf{x}) = \sum_{i=1}^{N} |S^i_{11\text{spec}} - S^i_{11\text{resp}}|^2 + \sum_{i=1}^{N} |S^i_{21\text{spec}} - S^i_{21\text{resp}}|^2, \quad (5)$$

where $S^i_{11\text{spec}}$ and $S^i_{21\text{spec}}$ are the desired scattering parameters and $S^i_{11\text{resp}}$ and $S^i_{21\text{resp}}$ are the computed scattering parameters

at the i-th frequency point in the k-th iteration while N is the number of frequency points.

Fig. 12 shows a typical starting point and the characteristics obtained using the zero-pole goal function and the goal function based on the scattering parameters.

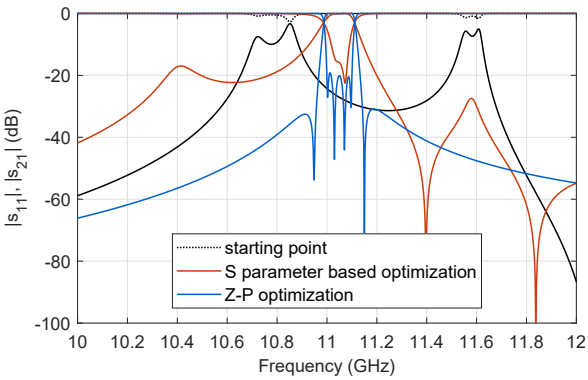

Fig. 12. Filter specification: f_c = 11.05 GHz, bandwidth 100 MHz, two transmission zeros at 10.95 and 11.15 GHz (-2.0778i and 2.0028i in the lowpass prototype domain), return loss level: 20 dB.

Table III shows the number of successful simulations for each of the three filter specifications. For the cost function of (5), the performance of the optimizer was very poor: it succeeded in only 6.3% of the cases. So here we indeed need to perform dimensional synthesis to get to a good starting point. However, the story is totally different with the zero-pole technique: all we need to do is click the start button, wait a few moments—*et voilà!* The optimization converges in all cases! Sometimes a little help is needed: the numbers in parentheses are the number of simulations that converged after extending the parameter variation ranges. Nevertheless, the robustness of the zero-pole optimizer combined with the mesh-morphing is amazing. Welcome to the designer's paradise (almost)!

TABLE III
THE NUMBER OF SUCCESSFUL TRIALS FOR EACH OF THREE FILTER SPECIFICATIONS.

	number of trials	number of successful trials	
		zero-pole	standard
Design 1	100	100 (5)	3 (2)
Design 2	100	100 (6)	9 (7)
Design 3	100	100 (14)	7 (1)
summary	300	300	19 (6.3%)

The final piece of information is the number of iterations involved in the zero-pole technique; this is shown for design 2 in Fig. 13. The height of each bar is the number of trials that converged in a given number of iterations. On average, 15.4 iterations were needed and the median was 13.5.

B. Fifth-order filter with dispersive couplings

The next example is a linear-phase waveguide filter with three frequency-dependent couplings, as described in [82]. This is a fifth-order filter that consists of a triplet featuring one strongly dispersive cross-coupling with negative slope

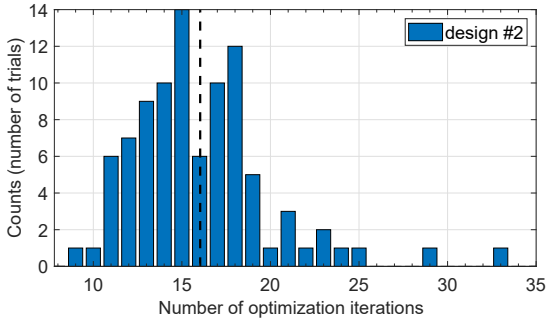

Fig. 13. Distribution of the number of optimization iterations for design 2 and the zero-pole approach. The average number of optimization iterations was 15.4 and the median was 13.5.

that is coupled (via partial height posts, giving frequency-dependent couplings with positive slope) to two resonators at the input and output. The coupling with the negative slope is implemented as a series stub. The dispersive couplings introduce four transmission zeros—a complex pair and two imaginary ones. The goals for the design are as follows: center frequency 9.98 GHz, bandwidth 320 MHz (3.21%), return loss level 20 dB, and imaginary transmission zeros at 9.66 GHz and 10.3 GHz. The complex zeros are located at 1.5+j9.98e9 and -1.5+j9.98e9. A total of fifteen design variables are taken into account in the optimization process: the lengths of five resonators (R_1, R_2, R_3, R_4, R_5), the length of the stub (L_1) and the length of the septum (L_2), the lengths and the positions of two partial-height posts (four design variables - p_1, p_2, d_1, d_2), two parameters controlling input/output coupling (l_1, l_4), and two parameters controlling coupling between the third resonator and the second and the fourth (l_2, l_3).

This filter is more challenging than the first one because it has flat-group delay requirements and there are dispersive couplings, which limits the choice of the goal function. Since there are complex transmission zeros, the goal function based on features cannot be used. The goal function involving a coupling matrix would require a special extraction procedure that accounts for frequency-dependent terms (such a procedure could be developed using the synthesis technique described in [83] or [84]). We will thus use the zero-pole approach, where there is no need to treat the optimization filters with dispersive couplings in any special way.

The set of initial design parameters was [R_1=15.25, R_2=19.4, R_3=16.3, R_4=20.9, R_5=15.25, L_1=12.4, L_2=8.55, p_1=5.4, p_2=5.2, d_1=2.25, d_2=2.25, l_1=11.7, l_4=10.2, l_2=10.2, l_3=11.9] (all dimensions in mm). Fig. 15 shows the initial design and the result of the EM-based zero-pole optimization. The full-order model involved about 0.6 million degrees of freedom, and one simulation with fast frequency sweep took about 50 seconds on a desktop computer with an Intel Core i7-7820X 8-core processor running at 3.60 GHz and 64 GB RAM. Optimization converged in 26 iterations and during this process the design parameters changed from 1.3 to 14.4%. The dimensions of the final design are given in Fig. 14. The simulated response agrees very well with the measured results in [82].

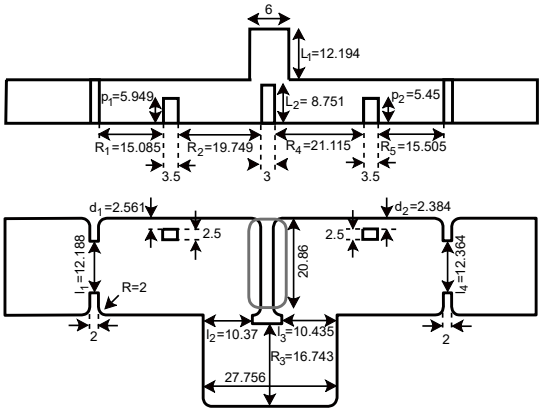

Fig. 14. A 3D view of the linear phase and side and top views, with the final dimensions found by optimization.

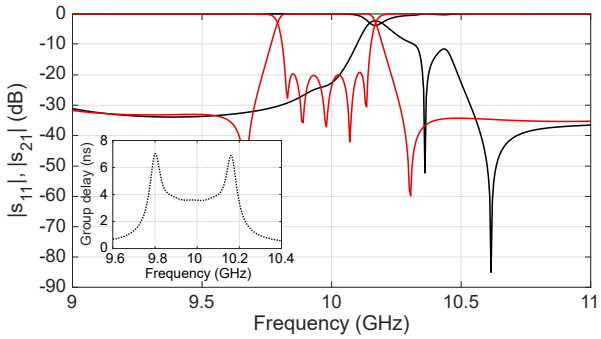

Fig. 15. Optimization of a fifth-order linear-phase filter with frequency dependent couplings: – initial design, – optimized design. The dimensions of the final design are given in Fig. 14. The simulated response agrees very well with the measured results in [82].

C. Dielectric resonator filter

We now move on to the most challenging example: the optimization of a sixth-order pseudoelliptic dielectric resonator filter with a 2.164–2.176 GHz passband, with 20 dB return loss, asymmetric response [54], and two transmission zeros located very close to each other at 2.162 and 2.163 GHz, resulting in very steep rejection. The filter structure is presented in the inset in Fig. 2. The simulated results are sensitive to meshing so this filter is very challenging; it is difficult even to simulate it with FEM or other numerical techniques, let alone optimize it. In the final design, two TZs and all six reflection zeros have to be resolved, which is not easy to achieve. Note that the separation between the zeros is just 1 MHz.

There were eighteen design variables: six screws controlling the resonant frequencies, four screws controlling the couplings (rotated 45 degrees), four parameters controlling the dielectric resonator spacing, two parameters controlling the input/output coupling, and two parameters controlling the iris dimensions (width and thickness).

To simulate this filter, we employed a server equipped with two Intel Xeon E5-2680 processors and a 256 GB RAM. The optimization process was carried out within the frequency interval from 2.12 to 2.2 GHz and involved two stages:

- Stage I: A coarse mesh was used, resulting in a problem with $\approx$ 0.65 million unknowns. To find the mesh, six iterations of adaptive mesh refinement were applied. In total, twelve iterations were needed to improve the initial design. The duration of this stage for three different solver setups (with or without deformation and different solver precision variants) are shown in Table IV. For the scenario without mesh morphing, six steps of mesh adaptation were performed at each iteration.
- Stage II: The solution obtained in Stage I was taken as a starting point. Stage II used only a double precision solver and mesh deformation. The fine mesh was computed in ten iterations of an adaptive mesh refinement process, resulting in a cumulative meshing time of 18.88 min. This produced a problem with $\approx$ 1.28 million unknowns. We then needed twenty iterations of a gradient-based optimizer, taking a total of 120 min, to reach the design goal.

The initial design, the design at the end of Stage I, and the final design are shown in Fig. 16 in black, blue, and red, respectively. Note that the reflection and transmission zeros are well resolved in the final design. The relative change in design parameters from the starting point to the final design was significant. In quantitative terms the changes were as follows: for the screws controlling the resonant frequencies – 23.1, 25.5, 19.2, 18.9, 24.2, and 23.6%, for the screws controlling the couplings – 6.0, 14.6, 8.9, and 0.7%, for the resonator spacing – 2.1,13.4, 8.5, and 3.6%, for the input/output coupling – 2.4 and 14%, and for the iris dimensions – 5 and 32.6%.

TABLE IV
STAGE I OF OPTIMIZATION SHOWING TOTAL TIME

Type	Duration
Double precision, no deformation	2 h 5 min 5 s
Double precision, with deformation	0 h 42 min 57 s
Mixed precision, with deformation	0 h 29 min 37 s

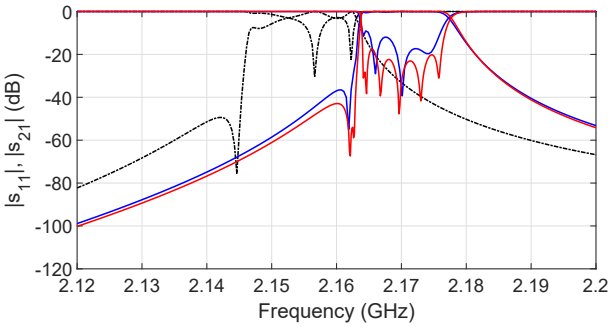

Fig. 16. Optimization of DR filter: – inital design, – first stage; – second stage.

V. WHAT'S NEXT ON THE HORIZON?

As we have shown, FEM-based optimization has reached a level where its computation no longer tests the patience of filter designers. With model-order reduction, mesh-morphing, and robust optimizers, EM-based CAD has become reasonably fast. Yet this is not the end of the process: more advances are coming that will further accelerate the process, giving

designers even more freedom in their choice of filter shape. Here we highlight a few of these developments.

The last row of Table IV presents the runtime for a mixed precision solver developed by our group. This solver performs certain operations in double precision, while others use single precision. This approach has two benefits: the computations proceed roughly 1.5 times faster, and they also need less memory. This mixed precision solver provides results with an accuracy that is almost equal to the results of the double precision analysis. The mixed precision curve coincides with the double precision curve except when the signal level is very low ($S_{21} < -100$dB).

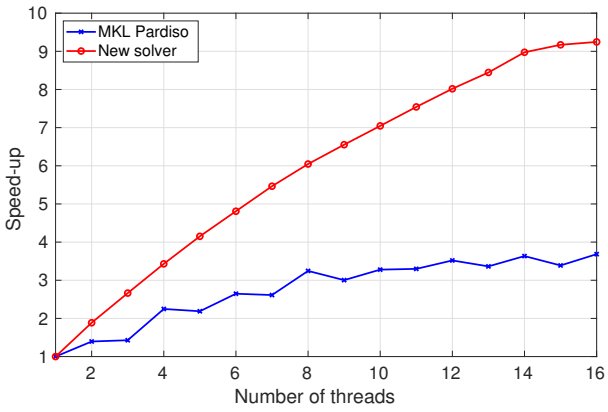

Fig. 17. Acceleration of MKL PARDISO and the new solver.

Numerical algorithms currently in use underutilize the computational capabilities of modern computer architectures. For instance, graphics processing units (GPUs) now contain thousands of cores. Electromagnetic simulators based on time-domain techniques like FD-TD make good use of these cores [85]; however, not much success has been reported to date in FEM. The benefits of using the extra processing power provided by GPUs can be seen in FEM matrix generation and assembly [86], [87], and in iterative solution of a sparse system of linear equations [87]–[90]. However, the sparse direct solvers needed for efficient MORe are yet to be developed. On the direct solver front, groups are also working on sparse solvers with reduced computational complexity [91], [92]. Additionally, there are efforts to develop new sparse direct solvers for many-core architectures [93]. Recent CPUs, such as Intel Xeons, support up to 56 cores. State-of-the art vendor libraries like Intel's MKL provide procedures for sparse matrix factorization. Intel MKL includes the PARDISO sparse solver which takes advantage of the multiple cores; however, its parallel efficiency is still limited, so new algorithms are needed to make better use of multiple cores. For instance, an early version of a new parallel algorithm developed in our group for sparse matrix factorization shows a better scalability than MKL PARDISO for a problem with about 1.4 million DoF and a server with two Intel Xeon E5-2687W processors (Fig. 17). As the number of cores in CPUs is likely to increase even further, scalable factorization techniques will allow faster speeds than have been seen in the current generation of solvers for sparse linear systems of equations.

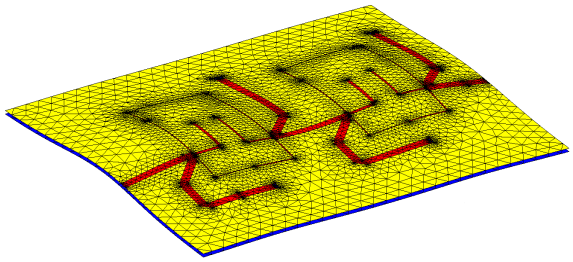

Fig. 18. 3D view of microwave filter after mesh deformation to fit a given surface.

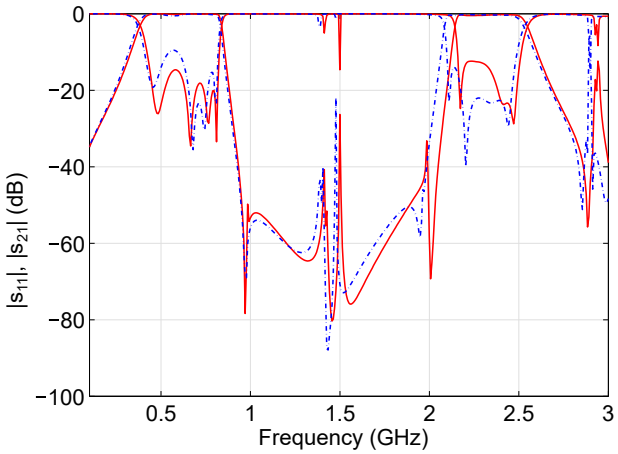

Fig. 19. Response of planar (red) vs. deformed (blue) filter versions.

Finally, another boost of at least an order of magnitude can be expected from the development of parametrized reduced-order models [65], [94]–[97].

Speed and optimization are important, but so are the shapes that filter designers can model in software. The numerical tools currently used in the industry allow the design of very complex geometries. However, in most cases the geometry is built from simple building blocks like boxes, cylinders, cones, and basic boolean operations on such objects. Anything that cannot be constructed from geometrical primitives is not available. This imposes severe constraints on the shapes that can be considered for electromagnetic simulations and design, preventing designers from exploring shapes that could actually be manufactured with (for example) additive manufacturing technology. Additive manufacturing allows for unconventional shapes to be used to improve the performance of the filters in SatCom and other applications [98]. As noted in the foreword to the Special Issue of the Proceedings of the IEEE on Additive Manufacturing of Radio-Frequency Components, improvements in software will be key in determining the speed at which additive manufacturing techniques will be introduced [99]. Finite-element-based software with mesh deformation techniques should enable advances in this area. Figs. 18 and 19 show an example of the capabilities of this approach. The substrate of the dualband filter considered earlier was placed on a deformed substrate (Fig. 18). This structure was then simulated in an FEM solver using its mesh deformation capabilities. The results for the planar and deformed versions

are given in Fig. 19.

VI. Takeaway

We hope that this article has demonstrated that some common beliefs regarding EM-based filter design are no longer valid, and in fact might be completely wrong. We offer the following (somewhat tongue-in-cheek) rules of thumb:

- An elegant optimization procedure should be able to find an acceptable solution, even without a good starting point.
- Brute-force optimization can be quite successful and it is often enough to feed the specification to an optimizer.

A final word of advice for filter designers: keep an eye out for the new generation of FEM solvers. They're just around the corner. Prepare for a bright future!

References

[1] D. Swanson and G. Macchiarella, "Microwave filter design by synthesis and optimization," *IEEE Microw. Mag.*, vol. 8, no. 2, pp. 55–69, Apr. 2007.

[2] M. Yu and Y. Wang, "Synthesis and beyond," *IEEE Microw. Mag.*, vol. 12, no. 6, pp. 62–76, Oct. 2011.

[3] J. Rubio, J. Arroyo, and J. Zapata, "Analysis of passive microwave circuits by using a hybrid 2-D and 3-D finite-element mode-matching method," *IEEE Trans. Microw. Theory Techn.*, vol. 47, no. 9, pp. 1746–1749, Sep. 1999.

[4] J.-M. Jin, *The Finite Element Method in Electromagnetics*, 3rd ed. New Jersey: John Wiley & Sons, 2014.

[5] S. Koziel, P. Kurgan, and B. Pankiewicz, "Cost-efficient design methodology for compact rat-race couplers," *Int. J. RF Microw. Comp. Aid. Eng.*, vol. 25, no. 3, pp. 236–242, Mar. 2015.

[6] I. Couckuyt, S. Koziel, and T. Dhaene, "Surrogate modeling of microwave structures using kriging, co-kriging, and space mapping," *Int. J. Numer. Model.: Electron. Devices Fields*, vol. 26, no. 1, pp. 64–73, Jan. 2013.

[7] N. Leszczynska, I. Couckuyt, T. Dhaene, and M. Mrozowski, "Low-cost surrogate models for microwave filters," *IEEE Microw. Wireless Compon. Lett.*, vol. 26, no. 12, pp. 969–971, Dec. 2016.

[8] A. Lamecki, L. Balewski, and M. Mrozowski, "Adaptive CAD-model construction schemes," *IEEE Trans. Magn.*, vol. 45, no. 3, pp. 1538–1541, Mar. 2009.

[9] Q.-J. Zhang, K. C. Gupta, and V. K. Devabhaktuni, "Artificial neural networks for RF and microwave design-from theory to practice," *IEEE Trans. Microw. Theory Techn.*, vol. 51, no. 4, pp. 1339–1350, Apr. 2003.

[10] J. E. Rayas-Sánchez, "EM-based optimization of microwave circuits using artificial neural networks: The state-of-the-art," *IEEE Trans. Microw. Theory Techn.*, vol. 52, no. 1, pp. 420–435, Jan. 2004.

[11] L.-Y. Xiao, W. Shao, X. Ding, and B.-Z. Wang, "Dynamic adjustment kernel extreme learning machine for microwave component design," *IEEE Trans. Microw. Theory Techn.*, no. 99, pp. 1–10, Oct. 2018.

[12] S. Koziel, Q. S. Cheng, and J. W. Bandler, "Space mapping," *IEEE Microw. Mag.*, vol. 9, no. 6, pp. 105–122, Dec. 2008.

[13] J. W. Bandler, Q. S. Cheng, S. A. Dakroury, A. S. Mohamed, M. H. Bakr, K. Madsen, and J. Sondergaard, "Space mapping: the state of the art," *IEEE Trans. Microw. Theory Techn.*, vol. 52, no. 1, pp. 337–361, Jan. 2004.

[14] J. E. Rayas-Sánchez, "Power in simplicity with ASM: tracing the aggressive space mapping algorithm over two decades of development and engineering applications," *IEEE Microw. Mag.*, vol. 17, no. 4, pp. 64–76, Apr. 2016.

[15] O. Lass, C. Posch, G. Scharrer, and S. Volkwein, "Space mapping techniques for a structural optimization problem governed by the p-Laplace equation," *Optim. Methods Softw.*, vol. 26, no. 4-5, pp. 617–642, Oct. 2011.

[16] T. Jansson, L. Nilsson, and M. Redhe, "Using surrogate models and response surfaces in structural optimization–with application to crash-worthiness design and sheet metal forming," *Struct. Multidiscip. Optim.*, vol. 25, no. 2, pp. 129–140, Jul. 2003.

[17] T. Robinson, M. Eldred, K. Willcox, and R. Haimes, "Surrogate-based optimization using multifidelity models with variable parameterization and corrected space mapping," *Aiaa J.*, vol. 46, no. 11, pp. 2814–2822, Nov. 2008.

[18] N. Leszczynska, A. Lamecki, and M. Mrozowski, "Fast full-wave multilevel zero-pole optimization of microwave filters," *IEEE Microw. Wireless Compon. Lett.*, vol. 26, no. 11, pp. 867–869, Nov. 2016.

[19] A. Lamecki, L. Balewski, and M. Mrozowski, "An efficient framework for fast computer aided design of microwave circuits based on the higher-order 3D finite-element method," *Radioengineering*, vol. 23, no. 4, pp. 970–978, Dec. 2014.

[20] G. Burke, E. Miller, S. Chakrabarti, and K. Demarest, "Using model-based parameter estimation to increase the efficiency of computing electromagnetic transfer functions," *IEEE Trans. Magn.*, vol. 25, no. 4, pp. 2807–2809, Jul. 1989.

[21] R. S. Adve, T. K. Sarkar, S. M. Rao, E. K. Miller, and D. R. Pflug, "Application of the Cauchy method for extrapolating/interpolating narrowband system responses," *IEEE Trans. Microw. Theory Techn.*, vol. 45, no. 5, pp. 837–845, May 1997.

[22] A. G. Lampérez, T. K. Sarkar, and M. S. Palma, "Generation of accurate rational models of lossy systems using the Cauchy method," *IEEE Microw. Wireless Compon. Lett.*, vol. 14, no. 10, pp. 490–492, Oct. 2004.

[23] S. F. Peik, R. R. Mansour, and Y. L. Chow, "Multidimensional Cauchy method and adaptive sampling for an accurate microwave circuit modeling," *IEEE Trans. Microw. Theory Techn.*, vol. 46, no. 12, pp. 2364–2371, Dec. 1998.

[24] Y. Ding, K.-L. Wu, and D. G. Fang, "A broad-band adaptive-frequency-sampling approach for microwave-circuit EM simulation exploiting Stoer-Bulirsch algorithm," *IEEE Trans. Microw. Theory Techn.*, vol. 51, no. 3, pp. 928–934, Mar. 2003.

[25] B. Gustavsen and A. Semlyen, "Rational approximation of frequency domain responses by vector fitting," *IEEE Trans. Power Del.*, vol. 14, no. 3, pp. 1052–1061, Jul. 1999.

[26] A. Mayo and A. Antoulas, "A framework for the solution of the generalized realization problem," *Linear Algebra Its Appl.*, vol. 425, no. 2-3, pp. 634–662, Sep. 2007.

[27] S. Lefteriu and A. C. Antoulas, "A new approach to modeling multiport systems from frequency-domain data," *IEEE Trans. Comput.-Aided Design Integr. Circuits Syst.*, vol. 29, no. 1, pp. 14–27, Jan. 2009.

[28] G. Antonini, D. Deschrijver, and T. Dhaene, "Broadband rational macromodeling based on the adaptive frequency sampling algorithm and the partial element equivalent circuit method," *IEEE Trans. Electromagn. Compat.*, vol. 50, no. 1, pp. 128–137, Feb. 2008.

[29] V. de la Rubia, U. Razafison, and Y. Maday, "Reliable fast frequency sweep for microwave devices via the reduced-basis method," *IEEE Trans. Microw. Theory Techn.*, vol. 57, no. 12, pp. 2923–2937, Dec. 2009.

[30] Y. Konkel, O. Farle, A. Köhler, A. Schultschik, and R. Dyczij-Edlinger, "Adaptive strategies for fast frequency sweeps," *COMPEL*, vol. 30, no. 6, pp. 1855–1869, Nov. 2011.

[31] V. de la Rubia, "Reliable reduced-order model for fast frequency sweep in microwave circuits," *Electromagnetics*, vol. 34, no. 3-4, pp. 161–170, Apr. 2014.

[32] M. Hess and P. Benner, "Fast evaluation of time harmonic Maxwell's equations using the reduced basis method," *IEEE Trans. Microw. Theory Techn.*, vol. 61, no. 6, pp. 2265–2274, Jun. 2013.

[33] R. Baltes, A. Schultschik, O. Farle, and R. Dyczij-Edlinger, "A finite-element-based fast frequency sweep framework including excitation by frequency-dependent waveguide mode patterns," *IEEE Trans. Microw. Theory Techn.*, vol. 65, no. 7, pp. 2249–2260, Jul. 2017.

[34] V. de la Rubia and M. Mrozowski, "A compact basis for reliable fast frequency sweep via the reduced-basis method," *IEEE Trans. Microw. Theory Techn.*, vol. 66, no. 10, pp. 4367–4382, Oct. 2018.

[35] L. T. Pillage, R. Rohrer *et al.*, "Asymptotic waveform evaluation for timing analysis," *IEEE Trans. Comput.-Aided Design Integr. Circuits Syst.*, vol. 9, no. 4, pp. 352–366, Apr. 1990.

[36] B. N. Sheehan, "ENOR: Model order reduction of RLC circuits using nodal equations for efficient factorization," in *Proc. IEEE 36th Design Autom. Conf.* ACM, Jun. 1999, pp. 17–21.

[37] A. Odabasioglu, M. Celik, and L. T. Pileggi, "PRIMA: passive reduced-order interconnect macromodeling algorithm," in *Proc. IEEE/ACM Int. Conf. Computer-Aided Design*. IEEE Computer Society, Aug. 1997, pp. 58–65.

[38] Y. Su, J. Wang, X. Zeng, Z. Bai, C. Chiang, and D. Zhou, "SAPOR: second-order Arnoldi method for passive order reduction of RCS circuits," in *Proc. Int. Conf. Comput.-Aided Design (ICCAD)*. IEEE Computer Society, Nov. 2004, pp. 74–79.

[39] D.-K. Sun, Z. Cendes, and J.-F. Lee, "ALPS-A new fast frequency-sweep procedure for microwave devices," *IEEE Trans. Microw. Theory Techn.*, vol. 49, no. 2, pp. 398–402, Feb. 2001.

[40] J. Rubio, J. Arroyo, and J. Zapata, "SFELP-an efficient methodology for microwave circuit analysis," *IEEE Trans. Microw. Theory Techn.*, vol. 49, no. 3, pp. 509–516, Mar. 2001.

[41] H. Wu and A. Cangellaris, "Krylov model order reduction of finite element models of electromagnetic structures with frequency-dependent material properties," in *IEEE MTT-Int, Microwave Symp.*, Jun. 2006, pp. 52–55.

[42] M. Rewienski, A. Lamecki, and M. Mrozowski, "Model order reduction for problems with dispersive surface boundary conditions," *IEEE Microw. Wireless Compon. Lett.*, vol. 25, no. 9, pp. 561–563, Sep. 2015.

[43] J. E. Bracken, D.-K. Sun, and Z. J. Cendes, "S-domain methods for simultaneous time and frequency characterization of electromagnetic devices," *IEEE Trans. Microw. Theory Techn.*, vol. 46, no. 9, pp. 1277–1290, Sep. 1998.

[44] Y. Zhu and A. C. Cangellaris, "A new finite element model for reduced order electromagnetic modeling," *IEEE Microw. Wireless Compon. Lett.*, vol. 11, no. 5, pp. 211–213, May 2001.

[45] H. Wu and A. C. Cangellaris, "Model-order reduction of finite-element approximations of passive electromagnetic devices including lumped electrical-circuit models," *IEEE Trans. Microw. Theory Techn.*, vol. 52, no. 9, pp. 2305–2313, Sep. 2004.

[46] G. Fotyga, K. Nyka, and M. Mrozowski, "Multilevel model order reduction with generalized compression of boundaries for 3-D FEM electromagnetic analysis," *Prog. Electromagn. Res.*, vol. 139, pp. 743–759, May 2013.

[47] G. Fotyga, M. Rewienski, and M. Mrozowski, "Wideband macromodels in finite element method," *IEEE Microw. Wireless Compon. Lett.*, vol. 25, no. 12, pp. 766–768, Dec. 2015.

[48] O. Farle, M. Lösch, and R. Dyczij-Edlinger, "Efficient fast frequency sweep without nonphysical resonances," *Electromagnetics*, vol. 30, no. 1-2, pp. 51–68, Mar. 2010.

[49] G. Fotyga, M. Czarniewska, A. Lamecki, and M. Mrozowski, "Reliable greedy multipoint model-order reduction techniques for finite-element analysis," *IEEE Antennas Wireless Propag. Lett.*, vol. 17, no. 5, pp. 821–824, May 2018.

[50] M. Rewienski, A. Lamecki, and M. Mrozowski, "Greedy multipoint model-order reduction technique for fast computation of scattering parameters of electromagnetic systems," *IEEE Trans. Microw. Theory Techn.*, vol. 64, no. 6, pp. 1681–1693, Jun. 2016.

[51] L. Feng, J. G. Korvink, and P. Benner, "A fully adaptive scheme for model order reduction based on moment matching," *IEEE Trans. Compon. Packag. Manuf. Technol.*, vol. 5, no. 12, pp. 1872–1884, Dec. 2015.

[52] M. Jemai and A. B. Kouki, "New adaptive multi-expansion frequencies approach for SP-MORe techniques with application to the well-conditioned asymptotic waveform evaluation," *IEEE Trans. Microw. Theory Techn.*, vol. 65, no. 10, pp. 3709–3719, Oct. 2017.

[53] R. D. Slone, R. Lee, and J.-F. Lee, "Multipoint Galerkin asymptotic waveform evaluation for model order reduction of frequency domain FEM electromagnetic radiation problems," *IEEE Trans. Antennas Propag.*, vol. 49, no. 10, pp. 1504–1513, Oct. 2001.

[54] S. Bastioli and R. V. Snyder, "In-line pseudoelliptic TE01d mode dielectric resonator filters," in *IEEE MTT-S. Int. Microw. Symp. Dig.* IEEE, Jun. 2012, pp. 1–3.

[55] M. Á. Sánchez-Soriano and R. Gómez-García, "Sharp-rejection wideband dual-band bandpass planar filters with broadly-separated passbands," *IEEE Microw. Wireless Compon. Lett.*, vol. 25, no. 2, pp. 97–99, Feb. 2015.

[56] W. Wang and M. N. Vouvakis, "Mesh morphing strategies for robust geometric parameter model reduction," in *Proc. IEEE Antennas Propag. Soc. Int. Symp. (APSURSI)*. IEEE, Jul. 2012, pp. 1–2.

[57] M. Rewienski, A. Lamecki, and M. Mrozowski, "A goal-oriented error estimator for reduced basis method modeling of microwave devices," *IEEE Microw. Wireless Compon. Lett.*, vol. 25, no. 4, pp. 208–210, Apr. 2015.

[58] S. Ratnajeevan, H. Hoole, K. Weeber, and S. Subramaniam, "Fictitious minima of object functions, finite element meshes, and edge elements in electromagnetic device synthesis," *IEEE Trans. Magn.*, vol. 27, no. 6, pp. 5214–5216, Nov. 1991.

[59] M. S. Berkani, S. Giurgea, C. Espanet, J.-L. Coulomb, and C. Kieffer, "Study on optimal design based on direct coupling between a FEM simulation model and L-BFGS-B algorithm," *IEEE Trans. Magn.*, vol. 49, no. 5, pp. 2149–2152, May 2013.

[60] M. Selim and R. Koomullil, "Mesh deformation approaches–a survey," *Journal of Physical Mathematics*, vol. 7, no. 2, 2016.

[61] M. L. Staten, S. J. Owen, S. M. Shontz, A. G. Salinger, and T. S. Coffey, "A comparison of mesh morphing methods for 3D shape optimization," in *Proc. 20th Int. Meshing Roundtable.* Springer, Oct. 2011, pp. 293–311.

[62] S. M. Shontz and S. A. Vavasis, "A mesh warping algorithm based on weighted Laplacian smoothing." in *IMR*, 2003, pp. 147–158.

[63] P. M. Bartier and C. P. Keller, "Multivariate interpolation to incorporate thematic surface data using inverse distance weighting (IDW)," *Computers & Geosciences*, vol. 22, no. 7, pp. 795–799, Aug. 1996.

[64] Y. Zhao and A. Forhad, "A general method for simulation of fluid flows with moving and compliant boundaries on unstructured grids," *Computer methods in applied mechanics and engineering*, vol. 192, no. 39-40, pp. 4439–4466, 2003.

[65] M. Czarniewska, G. Fotyga, A. Lamecki, and M. Mrozowski, "Parametrized local reduced-order models with compressed projection basis for fast parameter-dependent finite-element analysis," *IEEE Trans. Microw. Theory Techn.*, vol. 66, no. 8, pp. 3656–3667, Aug. 2018.

[66] B. Brandstatter, W. Ring, C. Magele, and K. R. Richter, "Shape design with great geometrical deformations using continuously moving finite element nodes," *IEEE Trans. Magn.*, vol. 34, no. 5, pp. 2877–2880, Sep. 1998.

[67] A. Mahanfar, S. Bila, M. Aubourg, and S. Verdeyme, "Mesh deformation techniques for geometrical optimization of microwave devices," in *Proc IEEE Antennas Propag Int Symp*, vol. 2. IEEE, Aug. 2003, pp. 56–59.

[68] A. Lamecki, "A mesh deformation technique based on solid mechanics for parametric analysis of high-frequency devices with 3-D FEM," *IEEE Trans. Microw. Theory Techn.*, vol. 64, no. 11, pp. 3400–3408, Nov. 2016.

[69] J. W. Bandler and S. H. Chen, "Circuit optimization: the state of the art," *IEEE Trans. Microw. Theory Techn.*, vol. 36, no. 2, pp. 424–443, Feb. 1988.

[70] R. J. Cameron, C. M. Kudsia, and R. Mansour, *Microwave filters for communication systems*. John Wiley & Sons, 2015.

[71] N. Aage and V. Egede Johansen, "Topology optimization of microwave waveguide filters," *International Journal for Numerical Methods in Engineering*, vol. 112, no. 3, pp. 283–300, Oct. 2017.

[72] D. G. Nielsen, S. D. Pedersen, V. Zhurbenko, V. E. Johansen, O. Sigmund, and N. Aage, "Topology optimization and experimental verification of compact E-plane waveguide filters," *Microw. Opt. Technol. Lett.*, pp. 1208–1215, May 2019.

[73] S. Koziel and J. W. Bandler, "Fast EM-driven design optimization of microwave filters using adjoint sensitivity and response features," in *2015 IEEE MTT-S International Microwave Symposium*. IEEE, 2015, pp. 1–3.

[74] C. Zhang, F. Feng, Q. J. Zhang, J. W. Bandler *et al.*, "Cognition-driven formulation of space mapping for equal-ripple optimization of microwave filters," *IEEE Trans. Microw. Theory Techn.*, vol. 63, no. 7, pp. 2154–2165, 2015.

[75] S. Bila, D. Baillargeat, M. Aubourg, S. Verdeyme, P. Guillon, F. Seyfert, J. Grimm, L. Baratchart, C. Zanchi, and J. Sombrin, "Direct electromagnetic optimization of microwave filters," *IEEE Microwave Magazine*, vol. 2, no. 1, pp. 46–51, 2001.

[76] P. Kozakowski and M. Mrozowski, "Quadratic programming approach to coupled resonator filter CAD," *IEEE Trans. Microw. Theory Techn.*, vol. 54, no. 11, pp. 3906–3913, 2006.

[77] A. Garcia-Lamperez, S. Llorente-Romano, M. Salazar-Palma, and T. K. Sarkar, "Efficient electromagnetic optimization of microwave filters and multiplexers using rational models," *IEEE Trans. Microw. Theory Techn.*, vol. 52, no. 2, pp. 508–521, Feb 2004.

[78] B. Thon, D. Bariant, S. Bila, D. Baillargeat, M. Aubourg, S. Verdeyme, P. Guillon, F. Thevenon, M. Rochette, J. Puech *et al.*, "Coupled Padé approximation-finite element method applied to microwave device design," in *2002 IEEE MTT-S International Microwave Symposium Digest (Cat. No. 02CH37278)*, vol. 3. IEEE, 2002, pp. 1889–1892.

[79] P. Kozakowski and M. Mrozowski, "Automated CAD of coupled resonator filters," *IEEE Microwave and Wireless Components Letters*, vol. 12, no. 12, pp. 470–472, 2002.

[80] N. Leszczynska, L. Szydlowski, and M. Mrozowski, "Zero-pole space mapping for CAD of filters," *IEEE Microwave and Wireless Components Letters*, vol. 24, no. 9, pp. 581–583, 2014.

[81] M. Guglielmi, P. Jarry, E. Kerherve, O. Roquebrun, and D. Schmitt, "A new family of all-inductive dual-mode filters," *IEEE Trans. Microw. Theory Techn.*, vol. 49, no. 10, pp. 1764–1769, Oct. 2001.

[82] L. Szydlowski and M. Mrozowski, "A self-equalized waveguide filter with frequency-dependent (resonant) couplings," *IEEE Microw. Wireless Compon. Lett.*, vol. 24, no. 11, pp. 769–771, Nov. 2014.

[83] L. Szydlowski, A. Lamecki, and M. Mrozowski, "Coupled-resonator waveguide filter in quadruplet topology with frequency-dependent

coupling–a design based on coupling matrix," *IEEE Microw. Wireless Compon. Lett.*, vol. 22, no. 11, pp. 553–555, Nov. 2012.
[84] L. Szydlowski, N. Leszczynska, and M. Mrozowski, "Generalized Chebyshev bandpass filters with frequency-dependent couplings based on stubs," *IEEE Trans. Microw. Theory Techn.*, vol. 61, no. 10, pp. 3601–3612, Oct. 2013.
[85] C. Y. Ong, M. Weldon, S. Quiring, L. Maxwell, M. C. Hughes, and M. Okoniewski, "Speed it up," *IEEE Microw. Mag.*, vol. 11, no. 2, pp. 70–78, Apr. 2010.
[86] A. Dziekonski, P. Sypek, A. Lamecki, and M. Mrozowski, "Generation of large finite-element matrices on multiple graphics processors," *Int. J. Numer. Methods Eng.*, vol. 94, no. 2, pp. 204–220, Apr. 2013.
[87] H.-T. Meng, B.-L. Nie, S. Wong, C. Macon, and J.-M. Jin, "GPU accelerated finite-element computation for electromagnetic analysis," *IEEE Antennas Propag. Mag.*, vol. 56, no. 2, pp. 39–62, Apr. 2014.
[88] A. Dziekonski and M. Mrozowski, "Block conjugate-gradient method with multilevel preconditioning and GPU acceleration for FEM problems in electromagnetics," *IEEE Antennas Wireless Propag. Lett.*, vol. 17, no. 6, pp. 1039–1042, Jun. 2018.
[89] A. Dziekonski, P. Sypek, A. Lamecki, and M. Mrozowski, "Communication and load balancing optimization for finite element electromagnetic simulations using multi-GPU workstation," *IEEE Trans. Microw. Theory Techn.*, vol. 65, no. 8, pp. 2661–2671, Aug. 2017.
[90] A. Dziekonski, A. Lamecki, and M. Mrozowski, "GPU acceleration of multilevel solvers for analysis of microwave components with finite element method," *IEEE Microwave and Wireless Components Letters*, vol. 21, no. 1, pp. 1–3, Jan. 2010.
[91] B. Zhou and D. Jiao, "Direct finite-element solver of linear complexity for large-scale 3-D electromagnetic analysis and circuit extraction," *IEEE Trans. Microw. Theory Techn.*, vol. 63, no. 10, pp. 3066–3080, Oct. 2015.
[92] M.-L. Yang, R.-Q. Liu, H.-W. Gao, and X.-Q. Sheng, "On the H-LU-based fast finite element direct solver for 3-D scattering problems," *IEEE Trans. Antennas Propag.*, vol. 66, no. 7, pp. 3792–3797, Jul. 2018.
[93] G. Pichon, E. Darve, M. Faverge, P. Ramet, and J. Roman, "Sparse supernodal solver using block low-rank compression: Design, performance and analysis," *J. Comput. Sci.*, vol. 27, pp. 255–270, Jul. 2018.
[94] M. Mul, V. de la Rubia, G. Fotyga, A. Lamecki, and M. Mrozowski, "Regularized local multivariate reduced-order models with nonaffine parameter dependence," *IEEE Trans. Microw. Theory Techn.*, vol. 67, no. 5, pp. 1778–1789, May 2019.
[95] A. Sommer, O. Farle, and R. Dyczij-Edlinger, "A new method for accurate and efficient residual computation in adaptive model-order reduction," *IEEE Trans. Magn.*, vol. 51, no. 3, pp. 1–4, Mar. 2015.
[96] S. Burgard, O. Farle, D. Klis, and R. Dyczij-Edlinger, "Order-reduction of fields-level models with affine and non-affine parameters by interpolation of subspaces," *IFAC-PapersOnLine*, vol. 48, no. 1, pp. 170–175, 2015.
[97] S. Clénet and T. Henneron, "Error estimation for model-order reduction of finite-element parametric problems," *IEEE Trans. Magn.*, vol. 52, no. 8, pp. 1–10, Aug. 2016.
[98] P. Booth and E. V. Lluch, "Enhancing the performance of waveguide filters using additive manufacturing," *Proc. IEEE*, vol. 105, no. 4, pp. 613–619, Apr. 2017.
[99] R. Sorrentino, P. Martin-Iglesias, O. A. Peverini, and T. M. Weller, "Additive manufacturing of radio-frequency components [Scanning the Issue]," *Proc. IEEE*, vol. 105, no. 4, pp. 589–592, Apr. 2017.